Estimating the depth and evolution of intrusions at resurgent calderas: Los Humeros (Mexico)

Stefano Urbani[1], Guido Giordano[1,2], Federico Lucci[1], Federico Rossetti[1], Valerio Acocella[1], Gerardo Carrasco- Núñez[3]
[1]Dipartimento di Scienze, Università degli Studi Roma Tre, L.go S.L. Murialdo 1, I-00146 Rome, Italy
[2]CNR - IDPA c/o Università degli Studi di Milano, Via Luigi Mangiagalli, 34, 20133 Milano
[3]Centro de Geociencias, Universidad Nacional Autónoma de México, Campus UNAM Juriquilla, 76100, Queretaro, Mexico

Correspondence to: Stefano Urbani (stefano.urbani@uniroma3.it)

Abstract. Resurgent calderas represent a target with high potential for geothermal exploration, as they are associated with the shallow emplacement of magma, resulting in a widespread and long lasting hydrothermal activity. Therefore, evaluating the thermal potential of resurgent calderas may provide important insights for geothermal exploitation. Resurgence is classically attributed to the uplift of a block or dome resulting from the inflation of the collapse-forming magma chamber due to the intrusion of new magma. The Los Humeros volcanic complex (LHVC; Mexico), consisting of two nested calderas (the outer Los Humeros and the inner, resurgent, Los Potreros), represents an area of high interest for geothermal exploration to optimize the current exploitation of the active geothermal field. Here we aim at better define the characteristics of the resurgence in Los Potreros, by integrating field work with analogue models, evaluating the spatio-temporal evolution of the deformation and the depth and extent of the intrusions responsible for the resurgence and which may represent also the local heat source(s).

Structural field analysis and geological mapping show that Los Potreros area is characterized by several lava domes and cryptodomes (with normal faulting at the top) that suggest multiple deformation sources localized in narrow areas.

The analogue experiments simulate the deformation pattern observed in the field, consisting of magma intrusions pushing a domed area with apical **depression**. To define the possible depth of the intrusion responsible for the observed surface deformations, we apply **tested** established relations **for elliptical sources to** our experiments **with sub-circular sources**. **We found that** these relations **are independent from the source and surface dome eccentricity and** suggest that the magmatic sources responsible for the deformation **in Los Potreros are** present at very shallow depths (hundreds of meters), which is in agreement with the well data and field observations. We therefore propose that the recent deformation at LHVC is not a classical resurgence associated with the bulk inflation of a deep magma reservoir; rather this is related to the ascent of shallow (<1 km) multiple magma bodies. A similar multiple source model of the subsurface structure has been also proposed for other calderas with an active geothermal system (Usu volcano, Japan) suggesting that the model proposed may have a wider applicability.

1 Introduction

Caldera resurgence consists of the **post-collapse** uplift of part of the caldera floor. **Resurgence has been described in several calderas worldwide (Smith and Bailey, 1968; Elston, 1984; Lipman, 1984 and references therein), representing a frequent step in caldera evolution. Several mechanisms have been invoked to trigger resurgence, including the pressurization of the hydrothermal system (Moretti et al., 2018), regional earthquakes (Walter et al., 2009), and magmatic intrusion (Kennedy et al. 2012). Discriminating the contributions to the observed uplift of each of these mechanisms is often challenging (Acocella, 2014). However, despite the possible hydrothermal**

and tectonic contributions, field observations in eroded resurgent calderas (e.g. Tomochic, Swanson and McDowell, 1985; Kutcharo, Goto and McPhie 2018; Turkey Creek, Du Bray and Pallister, 1999) coupled with the long timescale of the uplift of the caldera floor (from tens to thousands years), suggest that the intrusion of magmatic bodies is the prevalent mechanism for resurgence.

Resurgence is **commonly** attributed to the emplacement of silicic magmas at different depth levels under limited viscosity contrasts with regard to the previously emplaced magma (Marsh, 1984; Galetto et al., 2017). **However, though rare, resurgence may be also triggered by the injection of more primitive magma (Morán-Zenteno et al., 2004; Kennedy et al., 2012) or by the emplacement of basaltic sills, as recently documented at the Alcedo caldera (Galapagos; Galetto et al., 2019). The shape of the intracaldera resurgent structures is variable, being characterized by elliptical domes with longitudinal graben(s) at the top (e.g. Toba; De Silva et al., 2015; Snowdonia, Beavon, 1980; Timber Mountain, Christiansen et al., 1977) or, less commonly, by sub-circular domes (e.g. Cerro Galan, Folkes et al., 2011; Long Valley, Hildreth et al., 2017; Grizzly Peak, Fridrich et al., 1991) with both longitudinal grabens (Long Valley) or concentric fault blocks (Grizzly Peak) at their top.**

Whatever is the shape, resurgence is often associated with hydrothermal and ore forming processes, since the circulation pattern and temperature gradients of geothermal fluids are structurally-controlled by the space-time distribution of faults and fractures and by the depth and shape of the magmatic sources (e.g. Guillou Frottier et al., 2000; Prinbow et al., 2003; Stix et al., 2003; Mueller et al., 2009). Therefore, the characterisation of the magma that drives resurgence (location, depth and size) and of the factors controlling the release of the heat (permeability, fracture patterns, and fluid flow) have important implications for the exploration and exploitation of renewable geothermal energy resources. In particular, the estimation of the location, depth and geometry of the magmatic sources is crucial to define the geothermal and mineral potential of resurgent calderas, allowing an economically sustainable exploration and exploitation of their resulted natural resources.

The depth and size of the magmatic sources influences the deformation style of the resurgence at surface (Acocella et al., 2001). Deep sources (i.e. depth/diameter ratio ~1 assuming a spherical source) are associated to resurgent blocks (e.g. Ischia and Pantelleria, Acocella and Funiciello, 1999; Catalano et al., 2009), whereas shallower sources (i.e. depth/diameter ratio ~ 0.4) to resurgent domes (e.g. Valles and Yenkahe, Kennedy et al., 2012; Brothelande et al., 2016). Moreover, uplift rates may change by one order of magnitude form ~1 to ~10 cm per year (e.g. Yellowstone and Iwo Jima, Chang et al., 2007; Ueda et al., 2018). Nevertheless, despite showing different uplift styles and rates, these natural examples share a common feature that is a coherent uplift of the caldera floor.

This scenario differs from the occurrence of deformation patterns characterized by the widespread and delocalized uplift of several minor portions of the caldera floor, due to lava domes and/or cryptodomes, as observed at Usu volcano (Japan, Matsumoto and Nakagawa, 2010; Tomya et al., 2010). A different depth and extent of the responsible source(s) and, consequently, a different subsurface structure of the volcano is therefore suggested. A better assessment of the subsurface structure in such cases has crucial implications for geothermal exploration in order to maximize the geothermal production.

The Los Humeros Volcanic Complex (LHVC, Mexico) is an important geothermal target area, consisting of two nested calderas: **Los Humeros (the outer, larger and older one) and Los Potreros (the inner, smaller and younger one) (**Fig. 1). T**he latter is characterized by** the resurgence of **its floor, which was previously** interpreted as due to uplift **processes related** to the inflation of a several km deep magma chamber (Norini et al., 2015, **2019**).

This paper aims at (1) evaluating the depth **of** the intrusion(s) responsible for the uplift **in the LHVC area; (2)** explain the spatio-temporal evolution of the observed deformation of the caldera floor **and (3) test the validity of the linear relationship between the surface deformation structures and depth of elliptical sources (Brothelande and Merle 2015) for sub-circular sources.** To achieve **these** goals, we integrate results from structural field investigations carried out within the Los Potreros caldera with those derived from analogue experiments specifically designed to constrain the depth of the deformation source(s) in volcanic caldera environments. **The obtained** results **show that: (1) the relation between the source depth and surface deformation structures is independent from the source eccentricity; (2) the LHVC is characterized by** discontinuous and small-scale (**areal extent** ~ 1 km^2) surface deformations generated from multiple and shallow-**emplaced** (< 1 km **depth**) magmatic bodies. These results should be taken into account for **the** planning **of** future geothermal operations at the LHVC and in other calderas showing similar surface deformation.

2 Geological-structural setting

LHVC is located at the eastern termination of the Trans Mexican Volcanic Belt (TMVB, see inset in Fig. 1). The TMVB is the largest Neogene volcanic arc in Mexico (~1000 km long and up to ~300 km wide), **commonly associated with** the subduction of the Cocos and Rivera plates beneath the North American plate along the Middle American trench (Ferrari et al., 2012, and references therein). The LHVC consists of two nested calderas formed during the Pleistocene: the outer 18 x 16 km Los Humeros caldera and the inner 10 x 8 km Los Potreros caldera (Fig. 1, Ferriz and Mahood, 1984; Norini et al., 2015; Carrasco-Núñez et al., 2017b).

Based on updated stratigraphic and geochronological information, the evolution of the LHVC can be divided **into** three **main eruptive** stages (**Table 1,** Carrasco-Núñez et al., 2017b, 2018). Pre-caldera volcanism extended between ca. 700 and 164 ka (U-Th and $^{39}Ar/^{40}Ar$ dating**s in** Carrasco-Núñez et al., 2018), showing evidence for an extended building phase leading to the establishment of the large volume rhyolitic reservoir, **which fed several lava domes erupted to the western border of the Los Humeros Caldera**. **A** Caldera stage started at ca. 164 ka **(U-Th and $^{39}Ar/^{40}Ar$ ages, Carrasco-Núñez et al., 2018)**, with the eruption of the **115 km^3 Xaltipan ignimbrite that triggered** the collapse of the Los Humeros caldera**. This was followed by a Plinian eruptive episodic sequence, characterized by the emplacement of several rhyodacitic pumice fallout layers grouped as the Faby Tuff (Ferriz and Mahood, 1984). The Caldera stage** ended with the eruption of the 15 km^3 Zaragoza rhyodacite-andesite ignimbrite at **69±16 ka ($^{39}Ar/^{40}Ar$ ages, Carrasco-Núñez et al., 2018)** associated with the collapse of the nested Los Potreros caldera.

A post-caldera stage (< 69 ka) is interpreted by Carrasco-Núñez et al. (2018) **as composed by two main eruptive phases: (i)** a **late** Pleistocene resurgent phase, **characterized by the emplacement of silica-rich small domes and disperse explosive activity within Los Potreros caldera**, followed by **(ii)** Holocene basaltic to **trachytic** monogenetic, **intra-caldera and at the caldera-rim,** volcanism. This **eruptive behaviour indicates a change in the** configuration of the magmatic plumbing system **with respect to the early caldera stage of Los Humeros, which has been referred to** an unique, large and homogenized magma reservoir (e.g. Ferriz and Mohood, 1984; Verma, 1985)**. It is instead** in favour of a heterogeneous multi-layered system vertically distributed in the crust, with a deep (ca. 30 km **depth**) basaltic reservoir feeding progressively shallower and smaller distinct stagnation layers, pockets and batches up to very shallow conditions (ca. 3km) (Lucci et al., under review).

During the early resurgent phase of the **post-c**aldera stage, rhyolitic domes were emplaced along the northern rim of the Los Humeros caldera **and within the caldera at 44.8±1.7 ka (U-Th ages) and 50.7±4.4 ka ($^{39}Ar/^{40}Ar$ ages), respectively (Carrasco-Núñez et al., 2018). This effusive activity was followed by several explosive eruptions,**

which originated a dacitic air fall called Xoxoctic Tuff (0.6 km^3, Ferriz and Mahood, 1984) and a pyroclastic sequence that includes an explosive breccia and pyroclastic flow deposits comprising the Llano Tuff (Ferriz and Mahood 1984; Willcox, 2011).

The Holocene ring-fractures fed bimodal magmatism characterized by both explosive and effusive activity, producing several lava flows and domes, as well as the the ca. 7 ka (C-14 age, Dávila-Harris and Carrasco-Núñez, 2014) Cuicuiltic Member during periods of dominant explosive activity. It consists of alternating pumices and scoriae erupted during contemporaneous sub-Plinian to Strombolian activity from multiple vents located mostly along the inner part of the caldera and outer caldera ring faults (Dávila-Harris and Carrasco-Núñez, 2014). During this phase, less evolved lavas (trachyandesite to basalt) were erupted within and outside Los Humeros caldera, including the olivine-bearing basaltic lava that fills the previously formed Xalapasco crater (Fig. 1). Trachytic lava flows are the most recent activity recorded in the area, with an age of ca. 2.8 ka (C-14 age, Carrasco-Núñez et al., 2017b).

The reconstruction of the shallow stratigraphy within Los Potreros caldera is chiefly derived from the analysis of available well-logs (Figs. 2a-b Carrasco-Núñez et al., 2017a, b). Overall, the post-caldera units are lithologically dominated by lava flows resting on ignimbrite deposits emplaced during caldera stage. Ignimbrites of the caldera stage rest in turn on a thick sequence dominated by andesite lavas dated at ca. 1.4-2.8 Ma ($^{39}Ar/^{40}Ar$ ages, Carrasco-Núñez et al., 2017a). The subsurface geometry of the pre- and syn-caldera products is shown in Figs. 2a-b, where the in-depth geometry of the different magmatic products are cross-correlated and projected along the N-S and E-W direction, respectively. The N-S projection shows a constant depth of the top surface of the pre-caldera andesites that is associated with a highly variable depth (down to -400 m) of the top surface of the syn-caldera Xaltipan ignimbrite. The W-E projection shows a higher depth variability of both the top surface of the pre-caldera group (down to -500 m between H-19 and H-25 wells) and that of the Xaltipan ignimbrite (down to -400 m between H-19 and H-10 wells). Basaltic and rhyolitic-dacitic lavas occur at various depths (Carrasco-Núñez et al., 2017a); rhyolties-dacites are located mostly at the base (H-20 and H-26 wells) or within (H-05 well) the caldera group or the old andesite sequence (H-25 and H-19 wells). Basalts are located only within the pre-caldera andesite sequence, both at its base (in contact with the limestone basement; H-5 and H-8 wells) and at its top (in contact with the base of the caldera sequence; H-10 well). These bimodal lava products, showing an irregular lateral distribution, have been interpreted as subaerial (Carrasco-Núñez et al., 2017a).

The structural architecture of the LHVC is controlled by a network of active extensional fault systems, made of NNW-SSE, N-S, NE-SW and E-W striking fault strands cutting across the Los Potreros caldera floor. The following main faults were recognised (Norini et al., 2015, 2019; Calcagno et al., 2018) (Fig.1): (i) Maxtaloya (NNW-SSE striking), (ii) Los Humeros and Loma Blanca (N-S striking), (iii) Arroyo Grande (NE-SW striking), (iv) Las Viboras and Las Papas (E-W striking). Such active fault systems are interpreted as due to the recent/active resurgence of the Los Potreros Caldera. Since the faults do not show continuity beyond the caldera border, their scarps decrease in height towards the periphery of the caldera and the dip-slip displacement vectors show a semi-radial pattern (Norini et al., 2015).

The source of the areal uplift has been inferred to be the inflation of a saucer or cup shaped deep magmatic source elongated NNW-SSE, up warping a 8 x 4 km resurgent block, centred in the SE portion of the caldera, delimited to the W by the NNW–SSE main faults, and toward the north, east and south by the caldera rim (Fig.1, Norini et al., 2015, 2019).

The seismic activity between 1994-2017 is clustered along the Loma Blanca, Los Humeros and Arroyo Grande faults (Lermo et al., 2018; Fig. 1). Most of the earthquakes show a magnitude (Mw) between 1 and 2.5 and have been mainly interpreted as induced by the geothermal exploitation activity (injection of fluids and hydrofracturing; Lermo et al., 2018). Four major earthquakes (Mw= 3.2, 3.6, 3.9 and 4.2, at a depth of 1, 4, 2.2 and 1.8 km, respectively) have **also** been reported, with focal depths close to the trace of the active faults (Loma Blanca and Los Humeros, Fig.1). Such major earthquakes have been interpreted as triggered by fault reactivation due to fluid/brine circulation injected from geothermal wells (Lermo et al., 2018).

3 Methods

The scientific rationale adopted in this study is based on structural field work combined with analogue models aimed to constrain the depth of the deformation sources in the caldera domain. **We also tested if the relation that constrains the depth of the source deformation from surface parameters adopting elliptical sources (Brothelande and Merle 2015) is verified also for sub-circular sources.**

3.1 Structural field work

Structural field work was carried out **on the post-caldera (late Pleistocene to Holocene) deposits** to **characterise** the surface deformation related to the recent activity of the Los Potreros caldera **and constrain** the morphotectonic fingerprints of the resurgence **to evaluate its source and areal extent.** The geometry and distribution of the observable faults and joints were defined at the outcrop scale by measuring their attitudes (strike and dip; right-hand rule) and spacing. Fault kinematics was assessed through classical criteria on slickensides fault surfaces, such as Riedel shears**, growth fibers** and sheltering trails (Doblas, 1998). **The published geological map (Carrasco-Núñez et al., 2017b) and geothermal well data has been used (Carrasco-Núñez et al., 2017a) to correlate the surface structures at a broader scale.**

3.2 Analogue models: experimental set-up and scaling

Five experiments **were undertaken** simulating the ascent of a viscous **sub-circular** intrusion in a brittle overburden to test **the validity of** existing relationships between the depth of **elliptical intrusions** and the observed surface deformation **(Brothelande and Merle, 2015)**. The experimental set-up (Fig. **3**) consists of a 31 × 31 cm glass box filled with a sand pack (crust analogue) of variable thickness (T, of **10,** 30 and 50 mm, respectively). In each experiment we imposed a layering using a non-cohesive marine sand below a layer of crushed silica sand (grain size = 40-200 μm, cohesion = 300 Pa), fixing the thickness ratio of the two layers (T_u/T_l) to 1, to simulate the stratigraphy in Los Potreros (stiffer post caldera lava flows above softer and less cohesive ignimbrite deposits emplaced during the caldera collapse stage). At the base of the sand pack, a piston, controlled by a **motor**, pushes upward the silicone (magma analogue) placed inside a cylinder 8 cm in diameter. The injection rate is fixed for all the experiments to 2 mm/hr and each experiment was stopped at the onset of the silicone extrusion. Both sand and silicone physical properties are listed in Table **2**.

At the end of each experiment, the surface has been covered with sand to preserve their final topography and were **wetted** with water for cutting in sections to appreciate the subsurface deformation. Such sections were used to measure the mean dip of the **apical depression** faults (θ) induced by the rising silicone. A digital camera monitored the top view deformation of each experiment at 0.02 fps and a laser scanner, placed next to the camera, provided high-resolution data (maximum error ± 0.5 mm) of the vertical displacement that was used to measure in detail the geometrical features of the deformation i.e. dome diameter (L_d), **apical depression** width (L_g) and dome flank mean dip (α). According to the Buckingham-Π theorem (Merle and Borgia 1996 and references therein), our models need 7 independent dimensionless numbers to be properly scaled (i.e. 10 variables minus three dimensions; Table 2). Such dimensionless numbers can be defined as the ratios (Π) listed in Table 3. Some values of Π_5, representing the ratio between the inertial and viscous forces, are very small both in nature and experiments (1.3×10^{-20} and 6.1×10^{-10}, respectively), indicating that the inertial forces are negligible with respect to the viscous forces in both cases.

4 Results

4.1 Structural geology

The outcropping post-caldera lithologies within the Los Potreros Caldera consist of: (1) the Cuicuiltic Member, which blankets most of the surface of the upper half of the studied area; (2) basaltic lava flows filling the Xalapasco crater and the NW portion of the caldera; and (3) trachyandesitic and trachytic lava domes and thick flows extending in the southern half of the caldera and rhyolitic domes in its central part (Fig. 4). Field work documented that the more evolved lavas form five nearly N-S trending elliptical domes, distributed in both sides of the Los Humeros Fault (Figs. 4 and 5a): (i) a 2 km long × 1.2 km wide trachytic dome located to the west of the Maxtaloya and Los Humeros faults, (ii) a 1 × 0.7 km trachyandesitic dome located in a northeast area of the Maxtaloya fault, and (iii) one trachyandesitic and two obsidian smaller domes (0.4 × 0.2 km) to the eastern side of the Los Humeros Fault (LH-11 in Fig. 4).

Field work concentrated on the three main uplifted areas corresponding to the surface expression of the Loma Blanca, Arroyo Grande and Los Humeros faults (labelled LH1-2, LH9 and LH10 respectively in Fig. 4). The observed structures in these uplifted areas (joints and faults) affect the deposits of the post-caldera phase. Based on field evidence, we also propose a revised interpretation of the surface structures identified by previous studies (Norini et al., 2015, 2019), distinguishing between lineaments (morphological linear scarps, with no measurable fault offsets and/or alteration at the outcrop scale), active and inactive faults, instead associated with measurable fault offsets and with active or fossil alteration, respectively (Fig. 4). We present below a description of the structures mapped in the studied area, highlighting their temporal and spatial relationships with the post-caldera geological formations. We identified two inactive faults (Maxtaloya and Arroyo Grande), a morphological lineament (Las Papas) and two currently active faults (Los Humeros and Loma Blanca).

4.1.1 Las Papas lineament (sites LH-07, LH-08)

The E-W trending Las Papas lineament is localised within the Cuicuiltic Member (LH-07; Fig. 5b). We identified an erosional surface along the scarp, where unaltered and undeformed Cuicuiltic Member rocks rest above the Xoxoctic Tuff (LH-08, Fig. 5c). The E-W trending morphological lineament of Las Papas is probably due to differential erosion of the softer layers of the pyroclastic deposits, successively blanketed by the Cuicuiltic Member.

4.1.2 Arroyo Grande (site LH-09) and Maxtaloya scarps

The NE-SW Arroyo Grande scarp (Fig. 6a) exposes strongly altered and faulted (NW striking faults, mean attitude N144°/68°, number of data (*n*) = 8) lavas and ignimbrites unconformably covered by the unaltered Cuicuiltic Member (Fig.6b). The offset observed at the outcrop-scale for the single fault strands is ca. 0.5 m, with a dominant normal dip-slip kinematics (pitch angle of the slickenlines ranging 99°-106°). The inferred cumulative displacement at Arroyo Grande is ~ 10 m. Similarly, an outcrop on the Maxtaloya scarp (in front of well H-6) shows altered trachyandesites covered by unaltered Cuicuiltic Member rocks (Fig. 6c).

4.1.3 Los Humeros (site LH-10)

The fault scarp of the N-S striking (mean attitude N174°/73°, ***n*= 8**) Los Humeros Fault **exposes** the altered portions of the Cuicuiltic Member. Fault population analysis reveals a dominant normal dip-slip (mean pitch angle **of the slickenlines:** 84°) kinematics, as documented by both Riedel shears and carbonate-quartz growth steps. The main fault **surface** is sutured by a trachyandesitic extrusion (Fig. **6**d), localised along an aligned N-S dome (**site** LH-11 in Fig. **4**). Moreover, ~150 m southward from the outcrop of the fault scarp, a 5 × 3 m **wide** trachyandesitic plug shows vertical striation on its surface due to a subsurface vertical flow of the trachyandesite (Fig. **6**e). The observed displacement at the outcrop scale, as indicated by the height of the fault scarp, is ~ 10 m.

4.1.4 Loma Blanca (LH-01, LH-02)

The Loma Blanca **Fault** system (**sites** LH-01 and LH-02) is located in an active degassing area, where faults and fractures are frequent. The fault system **is** on top of an elongated crest (within an **apical depression**) of a morphological bulge, ~ 1 km in **width** and 30 m in height. At this location, the Cuicuiltic Member and the underlying trachyandesite lavas are strongly altered **(Fig. 6f)**. Evidence of stockwork veining and diffuse fracturing of the lavas suggests hydrofracturing and structurally controlled fluid flow and alteration. A set of NNE-SSW striking conjugate extensional faulting and jointing (joint spacing ~**0.5** m) is observed. The faults (mean attitude N26°/71°, ***n*= 6**) show a normal dip-slip kinematics (pitch **of the slickenlines** ranging 82°-104°). Joint systems found in the Cuicuiltic Member strike sub-parallel to the faults (mean attitude N37°/72°, *n*= 14). The inferred cumulative displacement of the faults, estimated by the depth of the apical **depression**, is ~ 5 m.

In summary, the 22 mapped faults in all the structural outcrops of the area show a main NNW-SSE strike (Fig. **6**g) with a dominant dip slip movement (mean pitch angle of slickenlines 88°, ***n*= 16**) which is sub-parallel to the N-S elongation of the lava domes and the Xalapasco crater.

4.2 Experimental results

Here we show **three representative** experiments with increasing overburden thickness (experiments **1-3-5 with T= 10, 30 and** 50 mm). Table **4** shows the measured parameters in the experiments. **Some experiments (1-2 and 3-4) were replicated with the same imposed boundary conditions and show the same result, which ensures model reproducibility.**

Overall, the experiments show a similar deformation pattern: a first stage characterized by the uplift of a sub-circular dome, bordered by inward dipping reverse faults, and a second stage characterized by the subsidence of the apical part of the dome where normal faulting occurs (**apical depression** formation Fig. **7**a-**i**). The reverse and normal faults are ring faults and are associated with the formation of radial fractures from the dome centre. **A different shape of the apical depression is observed with T/D > 0.12. In exp.1 (T/D = 0.12) an annular peripheral depression formed as the silicone reached the surface at the edge of the cylinder (Fig.7c). Conversely, in exp. 3 and 5 (T/D= 0.37 and 0.63 respectively) a sub-circular apical depression formed as the silicone reached the surface at the centre of the dome (Fig.7g, m).**

Despite the T/D ratio, all the experiments show that both the dome diameter and **apical depression** width increase linearly with the overburden thickness (ranging from **105** to 164 mm and from **14** to 58 mm respectively, Table **4**, **F**ig.**8**). The dome diameter increases abruptly with time, becoming almost constant at an early stage of the experiment (**F**ig.**9**a); the **apical depression** width shows a similar pattern even if it enlarges slightly with time (after the first abrupt increase) as the silicone rises towards the surface (Fig. 9b), suggesting that the intrusion depth has an higher influence on the **apical depression** width, in agreement with Brothelande and Merle (2015).

5. Discussion

5.1 Interpretation of the analogue experiments

The deformation pattern observed in the analogue experiments for thicker overburdens (experiments 3-4 and 5 with T/D= 0.37 and 0.63), showing a sub-circular dome and an apical depression, is in agreement with previous analogue experimental results (Acocella et al., 2001; Martì et al. 1994; Walter and Troll 2001). However, for thinner overburdens (exps. 1-2, T/D= 0.12), we observed a new deformation pattern at the surface consisting of an annular peripheral depression due to the rising of the silicone at the edge of the cylinder rather than its centre. We infer that in these experiments, since the rising silicone was very close to the surface, the sagging of the sand overburden pushed downward the centre of the silicone that squeezed up at the edges of the cylinder. Such process may also explain the two linear grabens that formed in the experiments with elliptical sources for small overburden thicknesses (ratio T/D ~ 0.1, Brothelande and Merle 2015).

The deformation pattern observed in our experiments is independent with respect to the imposed strain (i.e. uplift) rate or the viscosity of the intruding material as suggested by the similarity with results obtained in previous studies with higher strain rates (Acocella and Mulugeta, 2002) or lower viscosity intruding materials (Galetto et al., 2017; Martì et al. 1994; Walter and Troll, 2001). On the other hand, the occurrence of an apical depression is dependent on the thickness (i.e. depth) of the intrusion since thin intrusions relative to their depths will generate sub-circular domes without any apical depression (Galland et al., 2009; Galland, 2012). Moreover, our results confirm that the apical depression width shows a linear correlation with the source depth (Fig. 8) as estimated in Brothelande and Merle (2015) for elongated sources. This evidence documents that such relation is independent from the source eccentricity or shape of the extensional structures at the top of the dome (i.e. linear graben or sub-circular depression) suggesting that any elongation of the surface structure represents only a minor complication of the basic deformation pattern as already pointed out by (Roche et al., 2000).

5.2 Origin and extent of the resurgence in the LHVC

The distribution of the alteration patterns and deformation characteristics of the post caldera deposits can be used to infer the origin and extent of the uplift within the LHVC. In particular, **whether** the 7.4 ka Cuicuiltic Member **was invoved** in the deformation and alteration allow **constraining** the spatio-temporal evolution of the surficial deformation and associated uplifts in Los Potreros. Unaltered and undeformed deposits of the Cuicuiltic Member crop out along the E-W Las Papas lineament and unconformably cover altered and faulted lavas and ignimbrites along the Arroyo Grande and Maxtaloya scarps. Alteration and deformation of the Cuicuiltic Member occurs along the Los Humeros Fault scarp and within the apical **depression** of the Loma Blanca bulge. The vertical striations of the trachyandesitic plug near the Los Humeros fault scarp suggest that the ascent of the plug induced the uplift, the normal dip-slip faulting and alteration of the Cuicuiltic **Member**.

The observations suggest that Los Potreros is not a classic resurgent caldera (i.e. a caldera characterised by a large-scale process localized in a single area) but is characterised by a discontinuous uplift process in space and time, inducing small-scale deformations at each pulse (Fig. 10a-d). In particular, it was active in the south and north-eastern sector of the caldera, at Maxtaloya and Arroyo Grande (Fig. 10a), prior to the deposition of the Cuicuiltic Member (~ 7.4 ka), and then moved towards N along the Los Humeros and Loma Blanca scarps during and post the eruption of the

Cuicuiltic Member (Fig. 10b-d). The felsic lava found at the Los Humeros Fault scarp shows a similar mineral assemblage to the felsic domes located further south (Fig. 4); thus, the Los Humeros scarp may represent the final stage (i.e. effusive eruption of felsic magmas, (Fig. 10c) of the uplift process, which is thus driven by the ascent of relatively narrow (hundreds of meters) and highly viscous felsic magma batches. This is supported by the N-S elongation of the identified lava domes which is sub-parallel to the orientation of the measured fault planes (NNW-SSE), indicating that the observed deformation is closely related to the post-caldera volcanism. The ascent of such magma bodies is inferred here to drive the recent uplift and deformation of the Loma Blanca bulge, as suggested by the active fumaroles and extensive alteration of both the Cuicuiltic Member and post-caldera lavas (Fig. 10d). The presence of such shallow magma bodies is also suggested by the four major earthquakes recorded in Los Potreros, which have been previously interpreted to be induced by geothermal exploitation (Lermo et al., 2018). However, since the magnitude of the seismic events induced by geothermal exploitation activities is usually lower (i.e. < 3, Evans et al., 2012 and references therein), the higher magnitude (between 3.2 and 4.2) of the earthquakes in Los Potreros suggests that they may be more likely of volcano-tectonic origin due to shallow magma emplacement.

To further support the above interpretation from field observations, results from the presented analogue models were used to constrain the magma source depth from the geometrical parameters measured in the experiments (L_g, θ, α, Table 4). We calculated the theoretical overburden thickness (i.e. the intrusion depth, T_t, Table 4) as follow (Brothelande and Merle, 2015):

$$T_t = \frac{1}{2} L_g \times \frac{\sin(\theta+\alpha)}{\cos\theta} \quad (1)$$

Comparing the percentage difference (σ) between the imposed experimental (T) and theoretical (T_t) overburden thickness values, we calculate the associated error in the evaluation of the intrusion depth in the models (σ, Table 4, Fig.8). We then use equation (1) for the evaluation of the heat source depth at the Loma Blanca bulge considering σ ~ 40 % (maximum value of the experiments excluding those showing an annular depression that was not observed in the field). For the Loma Blanca bulge L_g= 286 m, θ= 71°, α= 4.5°, the estimated intrusion depth is 425 ± 170 m. Such relatively shallow depth is within the range of depths of rhyolitic-dacitic domes drilled in geothermal wells (spanning from 300 to 1700 m, Fig. 2a-b) and is consistent with the hypothesis that the uplift is driven by small and delocalized magmatic intrusions, as suggested by the field data.

The rhyolites-dacites have been previously interpreted of subaerial origin (Carrasco-Núñez et al., 2017a), but we suggest that at least some of them can be reinterpreted as intrusions of felsic cryptodomes based on the following considerations: (i) the occurrence of rhyolite-dacite lava bodies within the thick pre-caldera old andesite sequence is unusual and does not have a subaerial counterpart; (ii) the rhyolite body in well H-20 (Fig. 2b) up warps both the intracaldera ignimbrite sequence and the post-caldera lavas (showing a reduced thickness) indicating that the caldera forming ignimbrites do not level out the paleo-topography; and (iii) the top of the Xaltipan ignimbrite shows an higher depth variation than the pre caldera andesite (Fig. 2a) highlighting a local and discontinuous uplifting of the Xaltipan ignimbrite. Such evidence can be more easily reconciled with the intrusion of felsic cryptodomes within the volcanic sequence, rather than with a regular layer-cake stratigraphy.

5.3 Implications for the structure of the LHVC geothermal field

The combination of field and modelling data support that the uplift in Los Potreros caldera is due to multiple deformation sources in narrow areas that do not represent resurgence *sensu stricto*. Such localized recent deformation within Los Potreros caldera appears to be linked to small magmatic intrusions located at relatively shallow depths (i.e. < 1 km) as in Loma Blanca, where the estimated intrusion depth calculated from the experimental data is 425 ± 170 m.

This model differs from the general accepted idea of resurgence in Los Potreros induced by the inflation of a saucer or cup shaped deep magmatic intrusion (Norini et al., 2015, 2019). The resurgence is inferred to be centred beneath the sector of the caldera traversed by the E-W lineaments and limited by the Maxtaloya and Arroyo Grande faults (sector S1 in Norini et al., 2015). The thermal anomalies identified by Norini et al. (2015) show that the temperatures are unexpectedly cold beneath the inferred centre of the resurgent block, where the highest temperatures should be expected. By contrast, sharp and narrow temperature peaks, spatially coincident with Los Humeros and Loma Blanca faults, are consistent with the presence of shallow and delocalized heat sources. Indeed, the inflation of the deep magma chamber of the LHVC, inferred to be at 5 to 7-8 km of depth (Verma, 1983, 2000, 2011) and extending 9 km in radius and 6 km in length (thus coinciding with the Los Humeros caldera rim, Verma et al., 1990), should have resulted in a much wider uplift and with higher magnitude than the one observed in the field. Resurgence resulting from magma remobilization of the deep chamber that produced collapse is characterized by a larger-scale surface deformation (thousands of meters of uplift extending for tens of kilometers on the surface) as shown in many large calderas worldwide (Toba, de Silva et al., 2015; Cerro Galan, Folkes et al., 2011; Ischia, Carlino, 2012).

It is therefore unlikely that the replenishment of new magma in the caldera forming deep magma chamber accounts for the magnitude (few tens of meters) and discontinuous spatial distribution of the deformation in Los Potreros.

Such a model of the recent uplifting in Los Potreros is supported by field-based petrographic-mineralogical analysis showing that the present-day magmatic plumbing system is characterized by multiple magma levels spanning from a deep (30-33 km) basaltic reservoir to very shallow (~ 1.5 km), smaller, trachyandesitic-trachytic magma batches (Lucci et al., under review).

A similar model of the plumbing system has been proposed to explain the eruptive activity of Usu volcano (Japan) since 1663, a post caldera cone of the Toya caldera consisting of a basaltic main edifice surmounted by 3 felsic lava domes and more than 10 cryptodomes. Petrochemical data at Usu suggest the presence of multiple magma batches (i.e. sills) at 0.25-2 km deep that originated from partial melting of a metagabbro (Matsumoto and Nakagawa, 2010; Tomya et al., 2010).

Our proposed model has implications for planning future geothermal exploration: siting of future geothermal wells should consider that the presence of shallow heat sources within the caldera may complicate the pattern of isotherms associated with the deeper heat flow.

6 Conclusions

By integrating field work with analogue models, we constrain the late Pleistocene-Holocene spatio-temporal evolution of volcanism of the LHVC and estimate the depth of the magmatic intrusions feeding the active geothermal system. New findings on experimental analogue models of resurgent domes are also provided.

These are the main results that can be extracted from this study:

1. The distribution of the alteration patterns and deformation of the Cuicuiltic Member suggests that the recent (post-caldera collapse) uplift in Los Potreros caldera moved progressively northwards, from the south and north-eastern sector of the caldera towards N along the Los Humeros and Loma Blanca scarps.

2. The estimated depth of the intrusions responsible for such uplift is very shallow, as calculated from the experimental data for the Loma Blanca bulge (425 ± 170 m).

3. The recent uplift in Los Potreros is discontinuous in space and time, inducing small-scale (areal extent ~ 1 km^2) deformations originating from multiple and shallow (< 1 km depth) magmatic bodies, thus not representing a classic resurgent caldera, which usually involves large scale deformation (areal extent of several km^2).

4. The relation that relates the magmatic source depth with the surface parameters of resurgent domes is independent by the source eccentricity, similarly to what already verified for sub-circular intrusions.

Acknowledgements

CFE is kindly acknowledged for allowing work on the Los Humeros geothermal field. Federico Galetto helped for laser scanner data processing. Fabio Corbi and Matteo Trolese provided technical support in building the experimental set-up. Gianluca Norini is acknowledged for logistic support in the field. Alessandra Pensa kindly helped with figure drawings. Funded by the European Union's Horizon 2020 GEMex Project (grant agreement No. 727550) and by the Mexican Energy Sustainability Fund CONACYT-SENER, WP 4.5 of the Project 2015-04-268074. More information can be found on the GEMex Website: http://www.gemex-h2020.eu. The Grant to Department of Science, Roma Tre University (MIUR-Italy Dipartimenti di Eccellenza, ARTICOLO 1, COMMI 314 – 337 LEGGE 232/2016) is gratefully acknowledged.

References

Acocella, V.: Great challenges in volcanology: how does the volcano factory work?, Front. Earth Sci., 2:4, https://doi.org/10.3389/feart.2014.00004, 2014.

Acocella, V., and Funiciello, R.: The interaction between regional and local tectonics during resurgent doming: the case of the island of Ischia, Italy, J. Volcanol. Geoth. Res., 88, 109-123, https://doi.org/10.1016/S0377-0273(98)00109-7, 1999.

Acocella, V., and Mulugeta, G.: Experiments simulating surface deformation induced by pluton emplacement, Tectonophysics, 352, 275-293, https://doi.org/10.1016/S0040-1951(02)00218-4, 2002.

Acocella, V., Cifelli, F., and Funiciello, R.: The control of overburden thickness on resurgent domes, J. Volcanol. Geoth. Res., 111, 137–153, https://doi.org/10.1016/S0377-0273(01)00224-4, 2001.

Arellano, V.M., García, A., Barragán, R.M., Izquierdo, G., Aragón, A., and Nieva, D.: An updated conceptual model of the Los Humeros geothermal reservoir (Mexico), J. Volcanol. Geoth. Res., 124, 67–88, https://doi.org/10.1016/S0377-0273(03)00045-3, 2003.

Beavon, R.V.: A resurgent cauldron in the early Paleozoic of Wales, U.K., J. Volcanol. Geoth. Res., 7, 157-174, https://doi.org/10.1016/0377-0273(80)90025-6, 1980.

Brothelande, E., Peltier, A., Got, J.L., Merle, O., Lardy, M., and Garaebiti, E.: Constraints on the source of resurgent doming inferred from analogue and numerical modeling — Implications on the current feeding system of the Yenkahe dome–Yasur volcano complex (Vanuatu), J. Volcanol. Geoth. Res., 322, 225–240, https://doi.org/10.1016/j.jvolgeores.2015.11.023, 2016.

Brothelande, E., and Merle, O.: Estimation of magma depth for resurgent domes: An experimental approach, Earth Planet. Sc. Lett., 412, 143–151, https://doi.org/10.1016/j.epsl.2014.12.011, 2015.

Calcagno, P., Evanno, G., Trumpy, E., Carlos Gutiérrez-Negrín, L., MacIás, J.L., Carrasco-Núñez, G., and Liotta, D.: Preliminary 3-D geological models of Los Humeros and Acoculco geothermal fields (Mexico)-H2020 GEMex Project, Adv. Geosci., 45, 321–333, https://doi.org/10.5194/adgeo-45-321-2018, 2018.

Carlino, S.: The process of resurgence for Ischia Island (southern Italy) since 55 ka: The laccolith model and implications for eruption forecasting, B. Volcanol., 74, 947–961. https://doi.org/10.1007/s00445-012-0578-0, 2012.

Carrasco-Núñez, G., and Branney, M.J.: Progressive assembly of a massive layer of ignimbrite with a normal-to-reverse compositional zoning: The Zaragoza ignimbrite of central Mexico, B. Volcanol., 68, 3–20, https://doi.org/10.1007/s00445-005-0416-8, 2005.

Carrasco-Núñez, G., McCurry, M., Branney, M.J., Norry, M., and Willcox, C.: Complex magma mixing, mingling, and withdrawal associated with an intra-Plinian ignimbrite eruption at a large silicic caldera volcano: Los Humeros of central Mexico, Bull. Geol. Soc. Am., 124, 1793–1809, https://doi.org/10.1130/B30501.1, 2012.

Carrasco-Núñez, G., López-Martínez, M., Hernández, J., and Vargas, V.: Subsurface stratigraphy and its correlation with the surficial geology at Los Humeros geothermal field, eastern Trans-Mexican Volcanic Belt, Geothermics, 67, 1–17, https://doi.org/10.1016/j.geothermics.2017.01.001, 2017a.

Carrasco-Núñez, G., Hernández, J., De León, L., Dávila, P., Norini, G., Bernal, J.P., Jicha, B., Navarro, M., López-Quiroz, P., and Digitalis, T.: Geologic Map of Los Humeros volcanic complex and geothermal field, eastern Trans-Mexican Volcanic Belt, Terra Digitalis, 1, 1–11, https://doi.org/10.22201/igg.terradigitalis.2017.2.24.78, 2017b.

Carrasco-Núñez, G., Bernal, J.P., Dávila, P., Jicha, B., Giordano, G., and Hernández, J.: Reappraisal of Los Humeros volcanic complex by new U/Th zircon and 40Ar/39Ar dating: Implications for greater geothermal potential, Geochem. Geophy. Geosy., 19, 132-149, https://doi.org/10.1002/2017GC007044, 2018.

Catalano, S., De Guidi, G., Lanzafame, G., Monaco, C., and Tortotici, L.: Late quaternary deformation on the island on Pantelleria: new constraints for the recent tectonic evolution of the Sicily Channel Rift (southern Italy). J. Geodyn. 48, 75–82, 2009.

Chang, W.L., Smith, R.B., Wicks, C., Farrell, J.M., and Puskas, C.M.: Accelerated uplift and magmatic intrusion of the Yellowstone Caldera, 2004 to 2006, Science, 318, 952-956, https://doi.org/10.1126/science.1146842, 2007.

Christiansen, R.L., Lipman, P.W., Carr, W.J., Byers, F.M., Orkild, P.P., and Sargent, K.A.: Timber Mountain-Oasis Valley caldera complex of southern Nevada, Geol. Soc. Am. Bull., 88, 943-959, https://doi.org/10.1130/0016-7606(1977)88<943:TMVCCO>2.0.CO;2, 1977.

Dávila-Harris, P., and Carrasco-Núñez, G.: An unusual syn-eruptive bimodal eruption: The Holocene Cuicuiltic Member at Los Humeros caldera, Mexico, J. Volcanol. Geoth. Res., 271, 24–42, https://doi.org/10.1016/j.jvolgeores.2013.11.020, 2014.

de Silva, S.L., Mucek, A.E., Gregg, P.M., and Pratomo, I.: Resurgent Toba - field, chronologic, and model constraints on time scales and mechanisms of resurgence at large calderas, Front. Earth Sci., 3, 1–17, https://doi.org/10.3389/feart.2015.00025, 2015.

Doblas, M.: Slickenside kinematic indicators, Tectonophysics, 295, 187–197, https://doi.org/10.1016/S0040-1951(98)00120-6, 1998.

Du Bray, E.A., and Pallister, J.S.: Recrystallization and anatexis along the plutonic–volcanic contact of the Turkey Creek caldera, Arizona, Geol. Soc. Am. Bull., 111, 143–153, https://doi.org/10.1130/0016-7606(1999)111<0143:RAAATP>2.3.CO;2, 1999.

Elston, W.: Mid-Tertiary ash flow tuff cauldrons, southwestern New Mexico, J. Geophys. Res., 89, 8733–8750, https://doi.org/10.1029/JB089iB10p08733, 1984.

Evans, K.F., Zappone, A., Kraft, T., Deichmann, N., and Moia, F.: A survey of the induced seismic responses to fluid injection in geothermal and CO_2 reservoirs in Europe, Geothermics, 41, 30-54, https://doi.org/10.1016/j.geothermics.2011.08.002, 2012.

Ferrari, L., Orozco-Esquivel, T., Manea, V., and Manea, M.: The dynamic history of the Trans-Mexican Volcanic Belt and the Mexico subduction zone, Tectonophysics, 522–523, 122–149, https://doi.org/10.1016/j.tecto.2011.09.018, 2012.

Ferriz, H., and Mahood, G.A.: Eruption Rates and Compositional Trends at Los Humeros Volcanic Center, Puebla, Mexico, J. Geophys. Res., 89, 8511-8524, https://doi.org/10.1029/JB089iB10p08511, 1984.

Folkes, C.B., Wright, H.M., R.A.F. Cas, de Silva, S.L., Lesti, C., and Viramonte, J.G.: A re-appraisal of the stratigraphy and volcanology of the Cerro Galán volcanic system, NW Argentina, B. Volcanol., 73, 1427–1454, https://doi.org/10.1007/s00445-011-0459-y, 2011.

Fridrich, C.J., Smith, R.P., DeWitt, E., McKee, E.H.: Structural, eruptive, and intrusive evolution of the Grizzly Peak caldera, Sawatch Range, Colorado, Geol. Soc. Am. Bull., 103, 1160-1177, https://doi.org/10.1130/0016-7606(1991)103<1160:SEAIEO>2.3.CO;2, 1991.

Galetto, F., Acocella, V., and Caricchi, L.: Caldera resurgence driven by magma viscosity contrasts, Nat. Commun., 8, 1–11, https://doi.org/10.1038/s41467-017-01632-y, 2017.

Galetto, F., Bagnardi, M., Acocella, V., and Hooper, A.: Noneruptive unrest at the caldera of Alcedo Volcano (Galápagos Islands) revealed by InSAR data and geodetic modelling, J. Geophys. Res., 124, 3365–3381, https://doi.org/10.1029/2018JB017103, 2019.

Galland, O.: Experimental modelling of ground deformation associated with shallow magma intrusions, Earth Planet. Sc. Lett., 317-318, 145-156, https://doi.org/10.1016/j.epsl.2011.10.017, 2012.

Galland, O., Planke, S., Ragnhild Neumann, E., and Malthe-Sørenssen, A.: Experimental modelling of shallow magma emplacement: Application to saucer-shaped intrusions, Earth Planet. Sc. Lett., 277, 373-383, https://doi.org/10.1016/j.epsl.2008.11.003, 2009.

Goto, Y., and McPhie, J.: Tectonics, structure, and resurgence of the largest Quaternary caldera in Japan: Kutcharo, Hokkaido, Geol. Soc. Am. Bull., 130, 1307-1322, https://doi.org/10.1130/B31900.1, 2018.

Guillou-Frottier, L., Burov, E.B., and Milési, J.P.: Genetic links between ash-flow calderas and associated ore deposits as revealed by large-scale thermo-mechanical modelling, J. Volcanol. Geoth. Res., 102, 339–361, https://doi.org/10.1016/S0377-0273(00)00246-8, 2000.

Hildreth, W., Fierstein, J., and Calvert, A.: Early postcaldera rhyolite and structural resurgence at Long Valley Caldera, California, J. Volcanol. Geoth. Res., 335, 1-34, http://dx.doi.org/10.1016/j.jvolgeores.2017.01.005, 2017.

Kennedy, B., Wilcock, J., and Stix, J.: Caldera resurgence during magma replenishment and rejuvenation at Valles and Lake City calderas, B. Volcanol., 74, 1833–1847, https://doi.org/10.1007/s00445-012-0641-x, 2012.

Lipman, P. W.: The roots of ash flow calderas in Western North America: windows into the tops of granitic batholiths, J. Geophys. Res., 89, 8801–8841, https://doi.org/10.1029/JB089iB10p08801, 1984.

Lermo, J., Lorenzo, C., Jiménez, N., Ramos, E., Ângulo, J., Israel, J., Téllez, N., Machado, O., Álvarez, I., Torres, R., Alfaro R.: Analisis de la actividad sismica (1994-2016), su relacion con los pozos inyectores y productores y aplicación de nuevas tecnicas geofisica para caracterizar las zonas anómalas del campo geotérmico de Los Humeros, CEMIE-GEO, Mexico, Internal Rep., 42 pp., 2018.

Lucci, F., Carrasco-Núñez, G., Rossetti, F., Theye, T., White, J. C., Urbani, S., Azizi, H., Asahara, Y., and Giordano, G.: Anatomy of the magmatic plumbing system of Los Humeros Caldera (Mexico): implications for geothermal systems, Solid Earth Discuss., https://doi.org/10.5194/se-2019-86, in review, 2019.

Marsh, B.D.: On the mechanics of caldera resurgence, J. Geophys. Res., 89, 8245–8251, https://doi.org/10.1029/JB089iB10p08245, 1984.

Martì, J., Ablay, G.J., Redshaw, L.T., and Sparks, R.S.J.: Experimental studies of collapse calderas, J. Geol. Soc. London, 151, 919-929, https://doi.org/10.1144/gsjgs.151.6.0919, 1994.

Merle, O., Borgia, A.: Scaled experiments of volcanic spreading, J. Geophys. Res., 101, 13805-13817, https://doi.org/10.1029/95JB03736, 1996.

Morán-Zenteno, D.J., Alba-Aldave, L.A., Solé, J., and Iriondo, A.: A major resurgent caldera in southern Mexico: the source of the late Eocene Tilzapotla ignimbrite. J. Volcanol. Geoth. Res., 136, 97–119, https://doi.org/10.1016/j.jvolgeores.2004.04.002, 2004.

Moretti, R., Troise, C., Sarno, F., and De Natale, G.: Caldera unrest driven by CO2 induced drying of the deep hydrothermal system, Sci. Rep. UK, 8, https://doi.org/10.1038/s41598-018-26610-2, 2018.

Mueller, W.U., Stix, J., Corcoran, P.L., Daigneault, R.: Subaqueous calderas in the Archean Abitibi greenstone belt: An overview and new ideas, Ore Geol. Rev., 35, 4–46, https://doi.org/10.1016/j.oregeorev.2008.12.003, 2009.

Norini, G., Groppelli, G., Sulpizio, R., Carrasco-Núñez, G., Dávila-Harris, P., Pellicioli, C., Zucca, F., and De Franco, R.: Structural analysis and thermal remote sensing of the Los Humeros Volcanic Complex: Implications for volcano structure and geothermal exploration, J. Volcanol. Geoth. Res., 301, 221–237, https://doi.org/10.1016/j.jvolgeores.2015.05.014, 2015.

Norini, G., Carrasco–Núñez, G., Corbo-Camargo, F., Lermo, J., Hernández Rojas, J., Castro, C., Bonini, M., Montanari, D., Corti, G., Moratti, G., Chavez, G., Ramirez, M., and Cedillo F.: The structural architecture of the Los Humeros volcanic complex and geothermal field, J. Volcanol. Geoth. Res., 381, 312-329. https://doi.org/10.1016/j.jvolgeores.2019.06.010, 2019.

Matsumoto, A., and Nakagawa, M.: Formation and evolution of silicic magma plumbing system: Petrology of the volcanic rocks of Usu volcano, Hokkaido, Japan, J. Volcanol. Geoth. Res., 196, 185–207, https://doi.org/10.1016/j.jvolgeores.2010.07.014, 2010.

Pribnow, D.F.C., Schütze, C., Hurter, S.J., Flechsig, C., Sass, J.H.: Fluid flow in the resurgent dome of Long Valley Caldera: Implications from thermal data and deep electrical sounding. J. Volcanol. Geoth. Res., 127, 329–345, https://doi.org/10.1016/S0377-0273(03)00175-6, 2003.

Roche, O., Druitt, T.H., and Merle, O.: Experimental study of caldera formation, J. Geophys. Res., 105, https://doi.org/10.1029/1999JB900298, 395-416, 2000.

Smith, R. L., and Bailey, R. A.: Resurgent cauldrons, Geol. Soc. Am. Mem., 116, 613–662, https://doi.org/10.1130/MEM116, 1968.

Stix, J., Kennedy, B., Hannington, M., Gibson, H., Fiske, R., Mueller, W., Franklin, J.: Caldera-forming processes and the origin of submarine volcanogenic massive sulfide deposits, Geology, 31, 375–378, https://doi.org/10.1130/0091-7613(2003)031<0375:CFPATO>2.0.CO;2, 2003.

Swanson, E., and McDowell, F.: Geology and geochronology of the Tomochic caldera, Chihuahua, Mexico, Geol. Soc. Am. Bull., 96, 1477-1482, https://doi.org/10.1130/0016-7606(1985)96<1477:GAGOTT>2.0.CO;2, 1985.

Tomiya, A., Takahashi, E., Furukawa, N., Suzuki, T.: Depth and evolution of a silicic magma chamber: Melting experiments on a low-K rhyolite from Usu volcano, Japan, J. Petrol., 51, 1333–1354, https://doi.org/10.1093/petrology/egq021, 2010.

Ueda, H., Nagai, M., and Tanada, T.: Phreatic eruptions and deformation of Ioto Island (Iwo-jima), Japan, triggered by deep magma injection, Earth Planets Space, 70, https://doi.org/10.1186/s40623-018-0811-y, 2018.

Verma, M.P., Verma, S.P., and Sanvicente, H.: Temperature field simulation with stratification model of magma chamber under Los Humeros caldera, Puebla, Mexico, Geothermics, 19, 187–197, https://doi.org/10.1016/0375-6505(90)90015-4, 1990.

Verma, S.P., Gómez-Arias, E., and Andaverde, J.: Thermal sensitivity analysis of emplacement of the magma chamber in Los Humeros caldera, Puebla, Mexico, Int. Geol. Rev., 53, 905–925, https://doi.org/10.1080/00206810903234296, 2011.

Verma, S.P.: Magma genesis and chamber processes at Los Humeros caldera, Mexico - Nd and Sr isotope data, Nature, 302, 52–55, https://doi.org/10.1038/302052a0, 1983.

Verma, S.P.: Geochemical evidence for a lithospheric source for magmas from Los Humeros caldera, Puebla, Mexico. Chem. Geol. 164, 35–60, https://doi.org/10.1016/S0009-2541(99)00138-2, 2000.

Walter, T.R., and Troll, V.R.: Formation of caldera periphery faults: an experimental study, B. Volcanol., 63, 191-203, https://doi.org/10.1007/s004450100135, 2001.

Walter, T.R.,Wang, R., Acocella,V., Neri,M., Grosser, H.,and Zschau, J: Simultaneous magma and gas eruptions at three volcanoes in southern Italy: an earthquake trigger ?, Geology, 37, 251–254, https://doi.org/10.1130/G25396A, 2009.

Wilcox, C.P.: Eruptive, magmatic and structural evolution of a large explosive caldera volcano, Los Humeros, Central Mexico, Ph.D. thesis, Department of Geology, University of Leicester, United Kingdom, 317 pp., 2011.

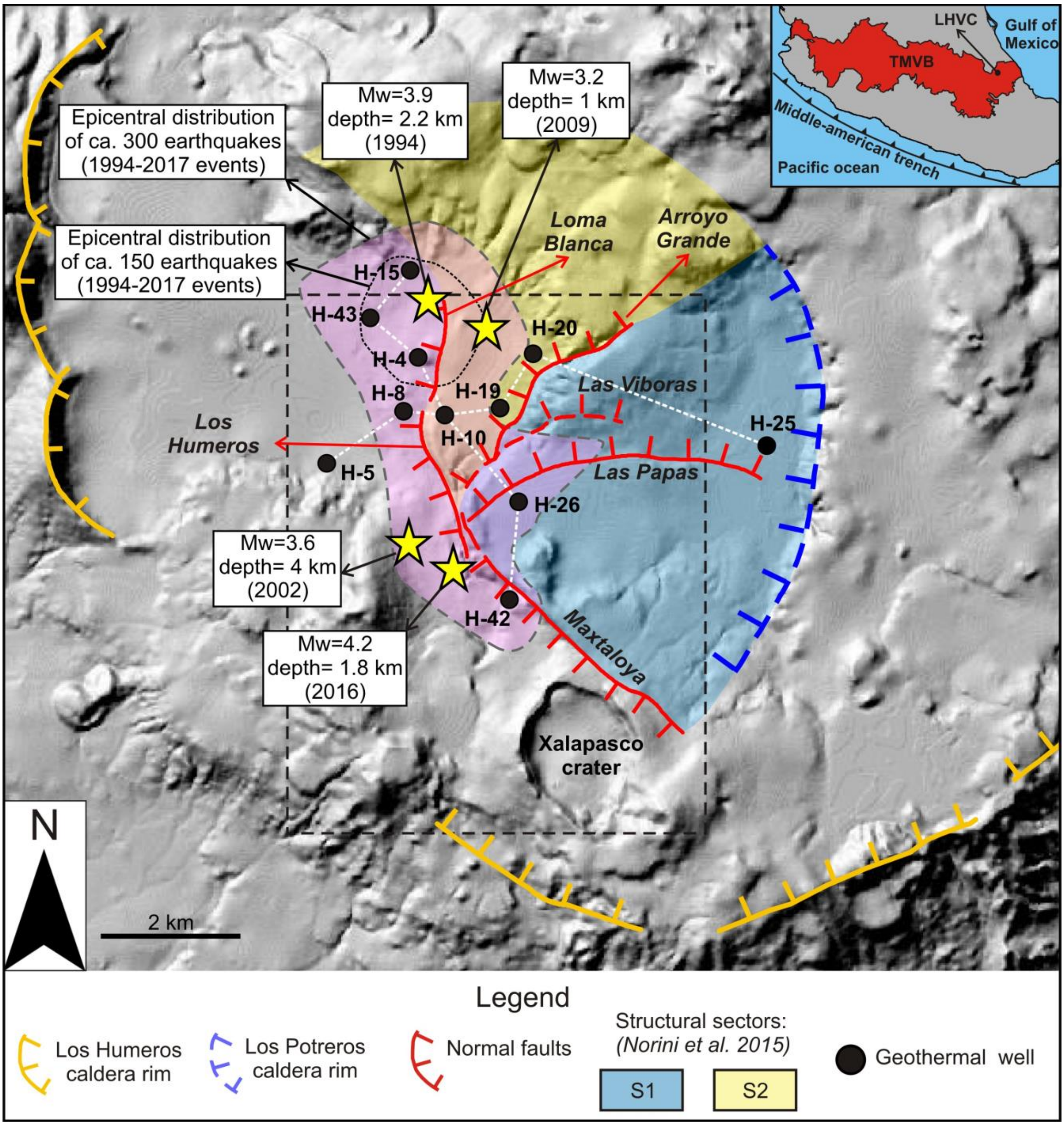

Figure 1: Shaded relief image (illuminated from the NE) obtained from 15 m resolution DEM of the Los Humeros Volcanic Complex (LHVC) showing the main structural features (faults and caldera rim, modified from Norini et al. (2015); Calcagno et al. (2018) and some geothermal wells referred in the text and in Figures 2a-b. The white dashed lines indicate the direction of the correlation sections shown in Figures 2a-b. The black rectangle indicates the studied area within the Los Potreros Caldera shown in Figure 4. The Inset box show the location of the LHVC (black dot and arrow) within the eastern sector of the Trans Mexican Volcanic Belt (TMVB). The structural sectors S1 and S2 correspond to the resurgent block inferred by Norini et al. (2015). Seismicity data from Lermo et al. (2018).

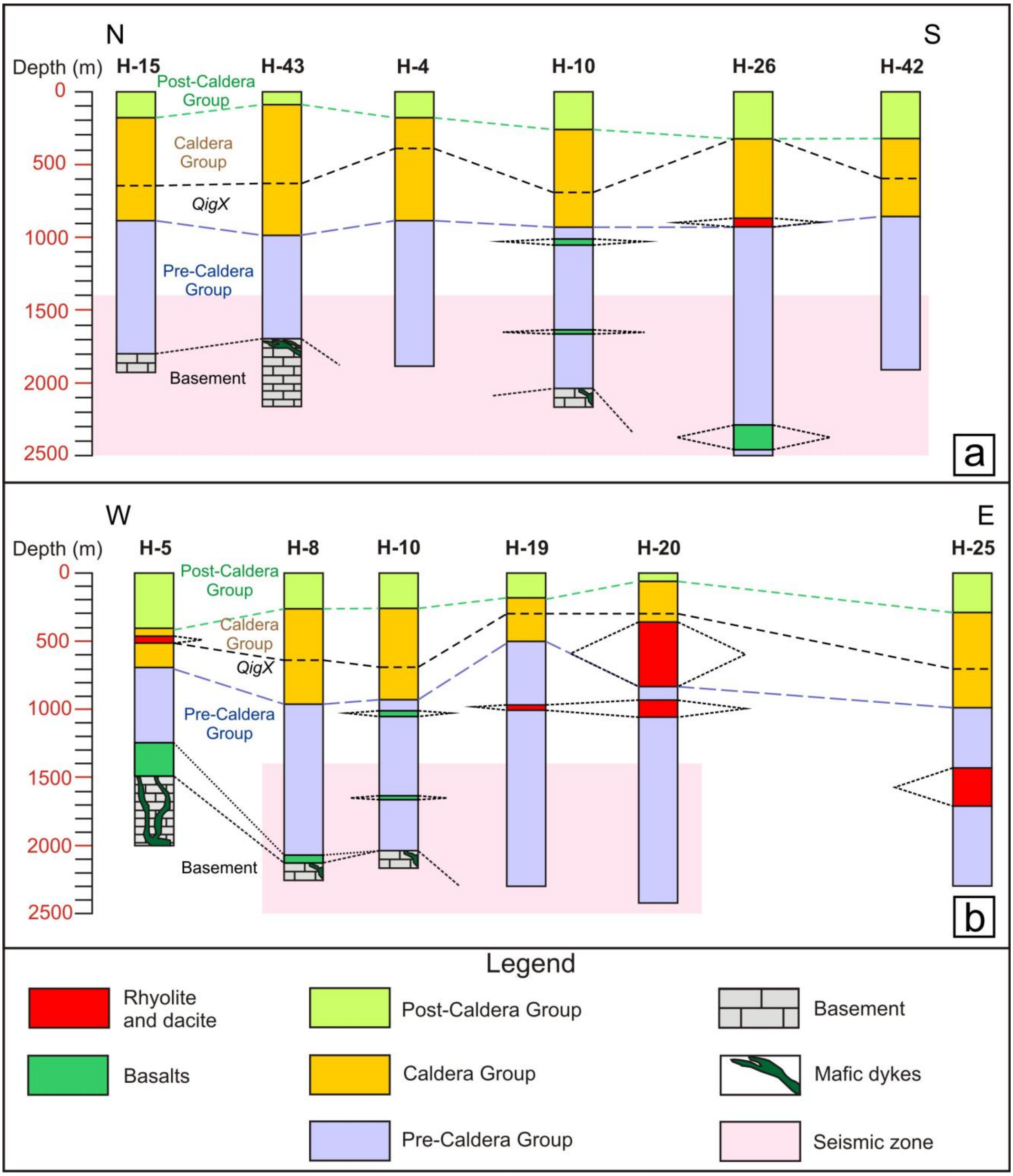

Figure 2: In depth correlation of lithostratigraphic units along the N-S (a) and W-E (b) direction (redrawn after Carrasco-Núñez et al. (2017a) and Arellano et al. (2003). Depth:horizontal distance=1:1. Location of the correlation line is shown in Figure 1. QigX= Xaltipan ignimbrite.

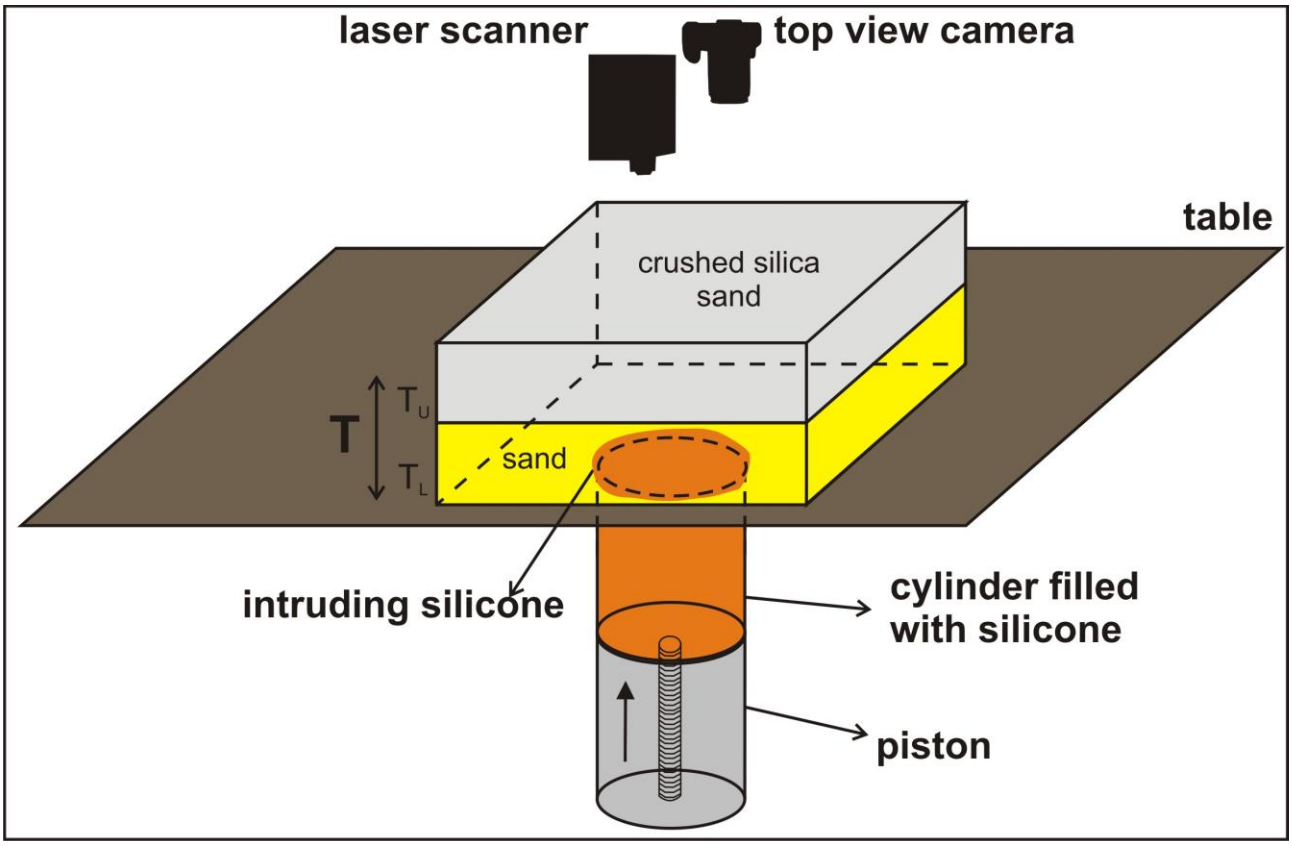

Figure 3: Experimental set-up. **A motor controlled piston pushes upward the silicone at a fixed rate (2mm/hr) from the base of the layered sand pack (the diameter of the silicone is 8 cm). A laser scanner and a camera record the surface deformation indiuced by the intruding silicone. T= total overburden thickness. T_U= upper layer thickness, T_L= lower layer thickness.**

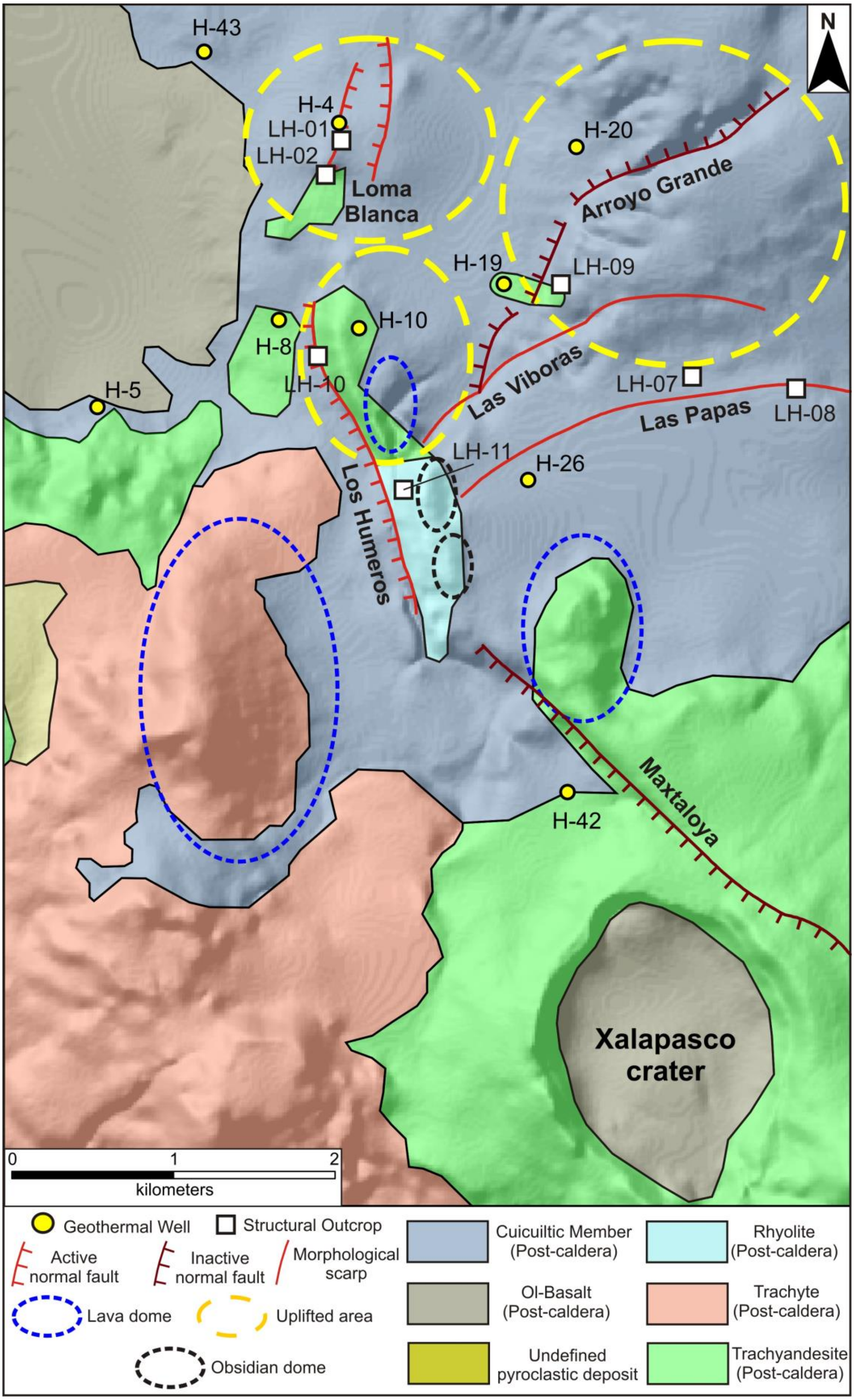

Figure 4: Simplified geological structural map of the studied area;reinterpreted after (Norini et al., 2015; Carrasco- Núñez et al., 2017b; Calcagno et al., 2018).

Figure 5: a) Panoramic view from Xalapasco crater (looking towards N) of the lava domes aligned N-S. b) Unaltered Cuicuiltic Member (LH-07). c) Unaltered Cuicuiltic Member covering a layered pyroclastic deposit, which can be laterally correlated with the Xoxoctic Tuff (LH-08). The erosional surface preceding the deposition of the Cuicuiltic Member is shown (dashed white line).

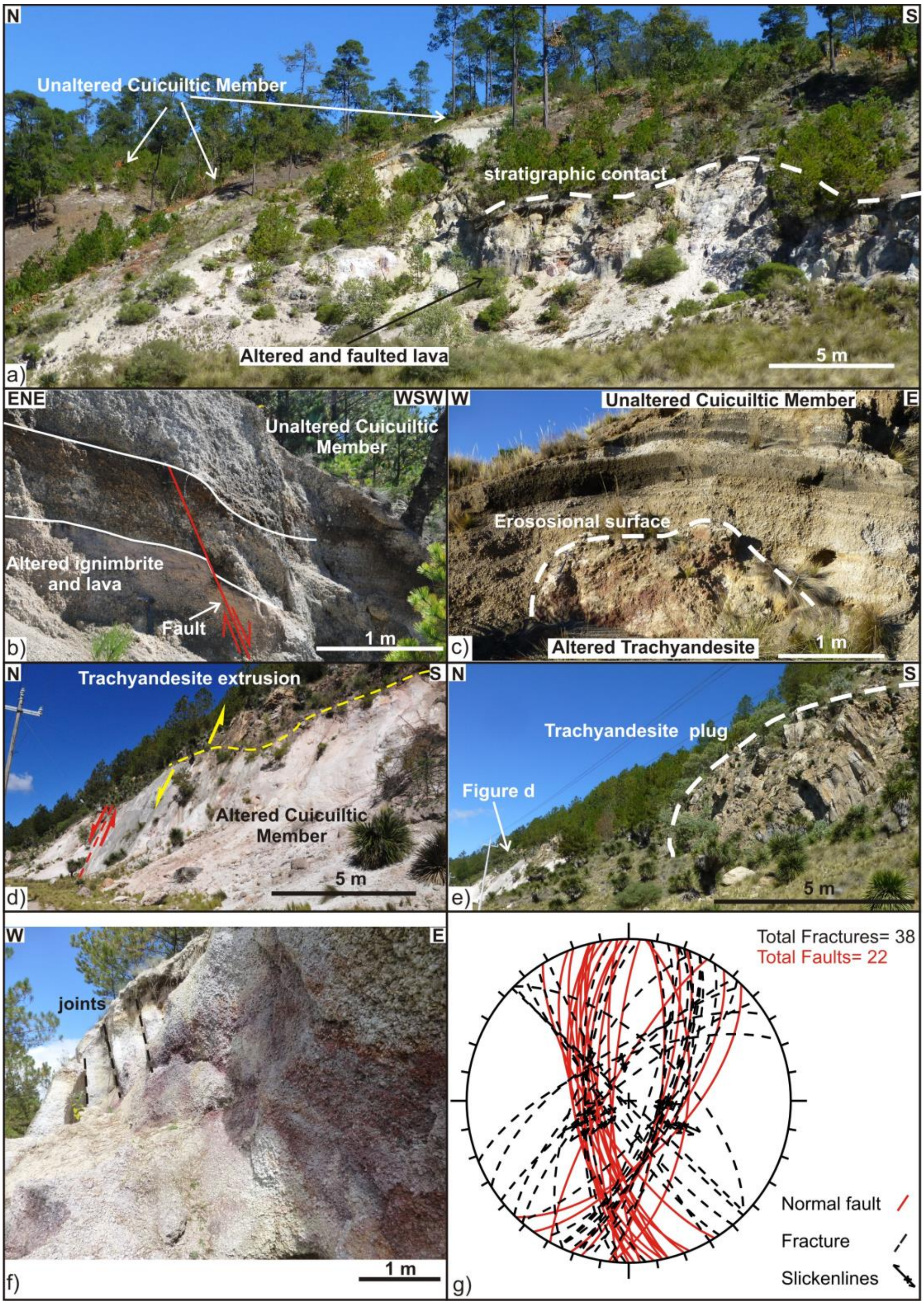

Figure 6: a) Panoramic view of the Arroyo Grande fault scarp showing the unaltered Cuicuiltic Member covering the altered and faulted ignimbrite and lavas (site LH-09). b) Normal fault affecting the altered ignimbrite deposits unconformably covered by the post-caldera, unaltered Cuicuiltic Member deposits (LH-09). Note that the Cuicuiltic Member deposits are not faulted at this location; the fault can be thus considered as a fossil fault with respect to the Cuicuiltic Member deposition. c) Block of altered trachyandesite buried by unaltered Cuicuiltic Member layers along the Maxtaloya fault scarp. d) Los Humeros fault scarp (LH-10) induced by the ascent of the trachyandesitic extrusion on top of the fault plane. e) Trachyandesite plug cropping out ~150 southward the fault scarp shown in d) (indicated by the red arrow). f) Jointing and alteration of the Cuicuiltic Member within the apical depression of the Loma Blanca dome (LH-01). e) Equal-area stereo-plot of the attitudes of faults and fractures in all the structural outcrops.

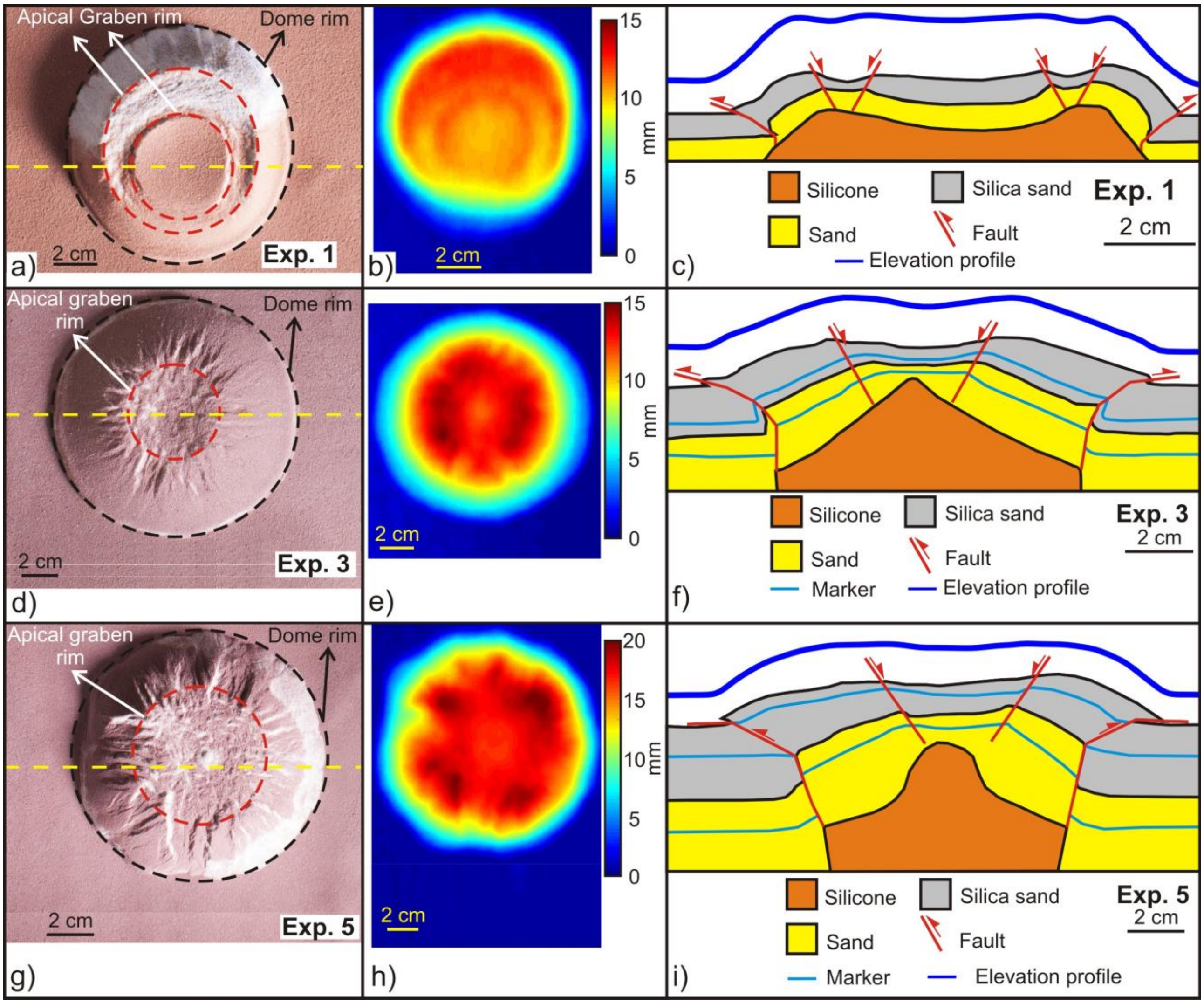

Figure 7: a) d) g) Top view image of the experiments 1, 3 and 5. b) e) h) cumulative vertical displacement; colour scale is proportional to the amount of uplift. c) f) i) Drawing of the cross section view obtained after cutting the section close to the dome center. The elevation profiles are obtained from laser scanner data. The yellow dashed line in a) d) g) indicates the trace of the section views and of the elevation profiles.

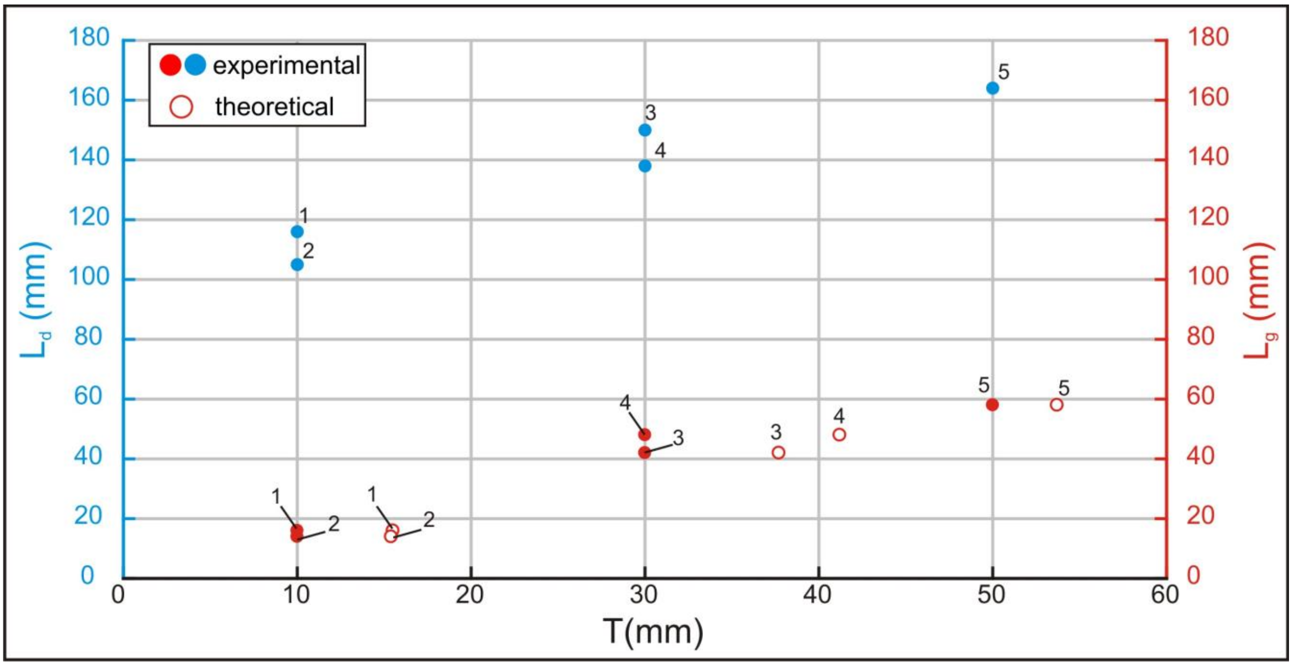

Figure 8: L_g (apical depression width) and L_d (dome diameter) versus T (overburden thickness). Theoretical values calculated after equation 1 (see discussion section). The numbers above each point indicate the experiment number.

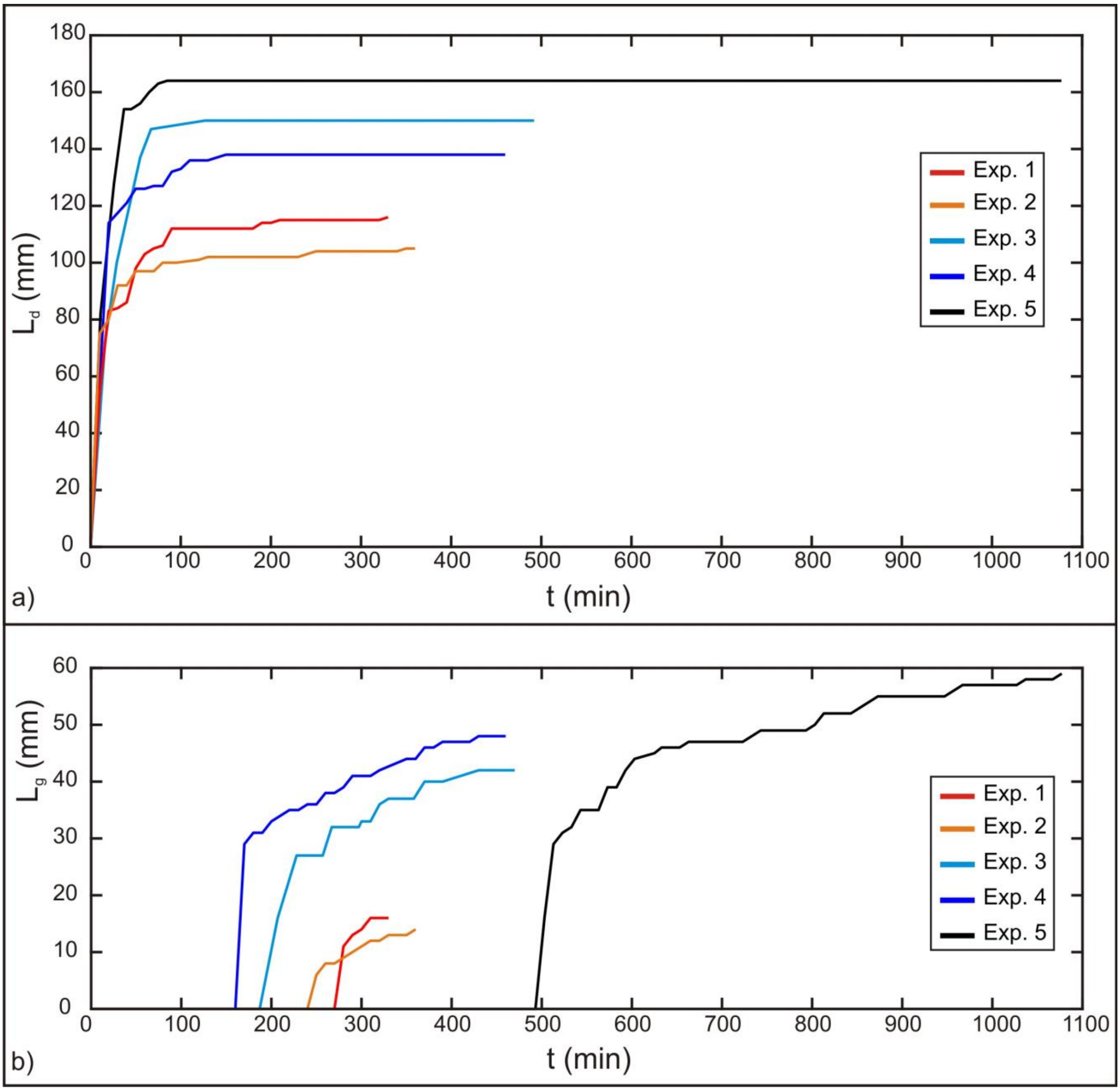

Figure 9: a) Time evolution of the dome diameter (L_d). b) Time evolution of the apical depression width (L_g). Both L_d and L_g show a similar evolution trend with a first stage of abrupt increase at the beginning of each experiment. In the second stage L_d becomes constant at t ~ 90 min (experiments 1-2-3), t ~ 150 min (experiment 4) and t ~ 65 min (experiment 5) while L_g increases slightly from t ~ 250-280 min (experiments 1-2), t ~ 210 min and ~ 170 min (experiments 3 and 4) and t ~ 530 min (experiment 5) till the end of the experiment.

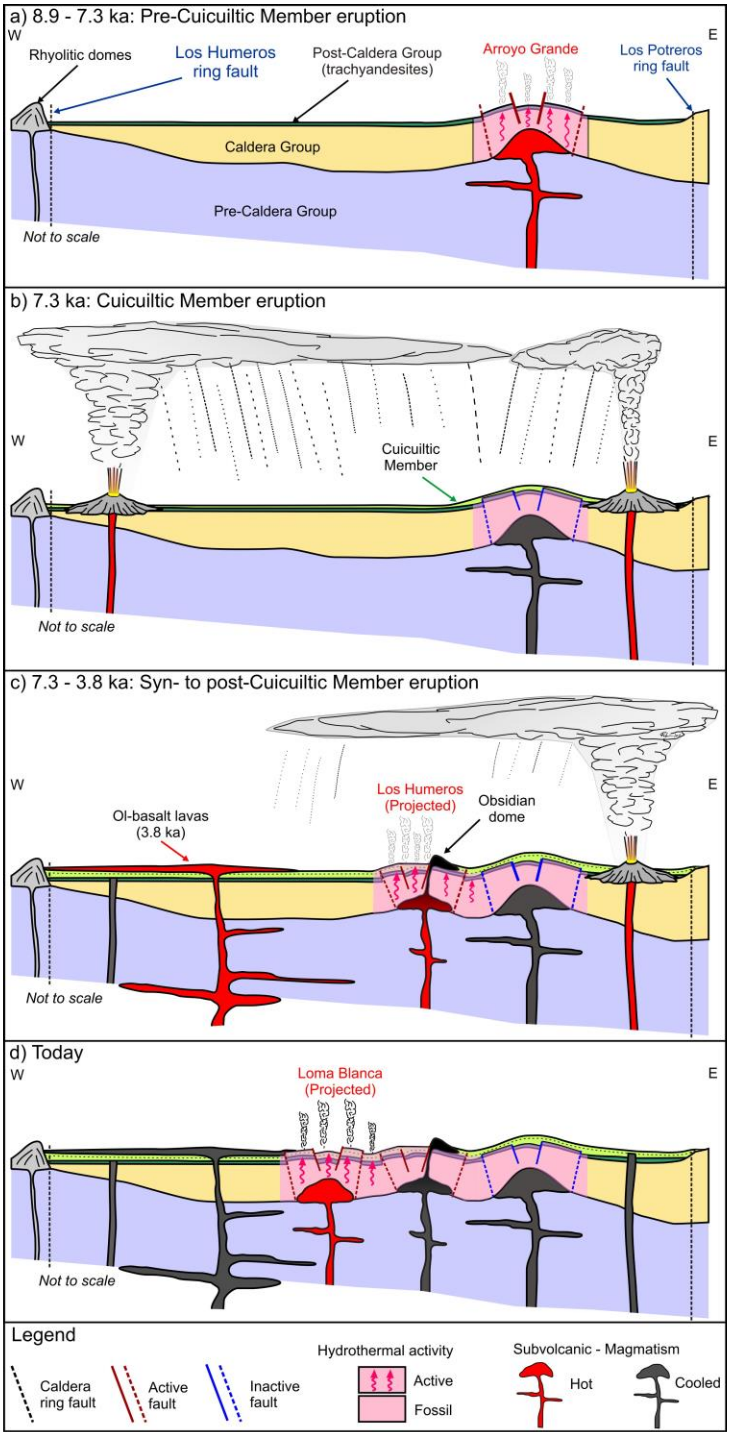

Figure 10: Schematic model of the evolution of the sub-surface structure of the Los Potreros caldera floor. Multiple magmatic intrusions located at relatively shallow depth (< 1 km) are responsible for the localized bulging of the caldera floor (Loma Blanca, Los Humeros and Arroyo Grande uplifted areas). a) Pre Cuicuiltic Member eruption: emplacement of a felsic intrusion at shallow depth and formation of the Arroyo grande bulge characterized by extensional faulting at its top, reverse faulting at its base and hydrotermalism. b) Cuicuiltic Member eruption: eruption of the Cuicuiltic Member covering the hydrothermally altered post-caldera trachyandesitic lavas. c) Syn to post Cuicuiltic Member eruption: formation of the Los Humeros fault and extrusion of obsidian lava domes along the fault scarp. As the trachyandesitic domes are covered with Cuicuiltic Member only at his base, the lava extrusion occurred during and post the Cuicuiltic Member eruption. d) Formation of the Loma Blanca bulge with the current hydrothermal activity and extensional faulting occurring within the apical depression. Notice that the emplacement of the succesive most recent domes (Los Humeros and Loma blanca) are not aligned on the same plane, they are shown for practical purposes.

Stage	Age (ka)	Main stratigraphic units
		Cuicuiltic Member and trachyandesitic to basaltic lavas
		Llano Tuff
		Xoxoctic Tuff
Post-caldera	< 69	Rhyolitic domes
		Zaragoza ignimbrite
		Faby Tuff
Caldera	164-69	Xaltipan ignimbrite
Pre-Caldera	700-164	Rhyolitic Domes

Table 1 Summary of the main stratigraphic units of the three evolutionary stages of the Los Humeros Volcanic complex (Carrasco-Núñez et al., 2017b, 2018).

Parameter	Definition	Value (experiments)	Value (nature)
T	Thickness of the overburden	1-5 X 10^{-2} m	300-2000 m
L_d	Dome diameter	1-1.6 X 10^{-1} m	2000 m
H	Dome height	1.1-2 X 10^{-2} m	100 m
ρ_s	Density of brittle overburden	1400 kg/m^3	2800 kg/m^3
ϕ	Angle of internal friction	35°	25-40°
τ_0	Cohesion (brittle overburden)	300 Pa	10^6 Pa
ρ_m	Density of intrusive material	1000 kg/m^3	2500 kg/m^3
μ_m	Viscosity of intrusive material	10^4 Pa s	10^{15} Pa s
g	Gravity	9.8 m/s^2	9.8 m/s^2
t	Timespan for deformation	2.8-6.5 X 10^4 s	1.9 X 10^{12} s

Table 2. Comparison of the geometric and material properties parameters of the experiments and nature.

Dimensionless ratio	Experiments	Nature
$\Pi_1 = T/L_d$	0.1-0.5	0.15–1
$\Pi_2 = H/L_d$	0.08-0.2	0.05-0.1
$\Pi_3 = \rho_s/\rho_m$	1.4	1.12
$\Pi_4 = \phi$	35	25-40
$\Pi_5 = \rho_m H^2/\mu_m t$	6.1 X 10^{-10}	1.3 X 10^{-20}
$\Pi_6 = \rho_m g H t/\mu_m$	1.3 X 10^3	4.6 X 10^3
$\Pi_7 = \rho_s g T/\tau_0$	2.3	8.24

Table 3. Definition and values of the dimensionless ratios Π in nature and in the experiments.

Exp	T (mm)	L_g (mm)	L_d (mm)	θ	α	T_t (mm)	σ (%)
1	10	16	116	58°	14°	15.5	55
2	10	14	105	63°	27°	15.4	54
3	30	42	150	58°	14°	37.7	27
4	30	48	138	56°	18°	41.2	37
5	50	58	164	58°	21°	53.7	7

Table 4. Measured (Lg, Ld, θ, α) and imposed (T) parameters in the experiments. T=overburden thickness; L_d= dome diameter; L_g= apical depression width; θ= apical depression fault dip; α= dome flank mean dip; T_t= theoretical overburden

thickness calculated with equation 1 (Brothelande and Merle, 2015, see discussion section); σ= percentage difference between T and T_t.